Sustainable Chemistry for the Environment 4 (2023) 100051

Contents lists available at ScienceDirect

Sustainable Chemistry for the Environment

journal homepage: www.editorialmanager.com/scenv

Effect of the physicochemical properties of bimetallic Ni-Cu catalysts for hydrogenation/hydrogenolysis of HMF varying the synthesis method

Nerea Viar [a,b,*], Jesus M. Requies [a], Tommaso Tabanelli [b], Fabrizio Cavani [b], Ane Bueno [a], Mikel Oregui Bengoechea [a]

[a] Chemical and Environmental Engineering Department, Engineering Faculty of Bilbao, University of the Basque Country (UPV/EHU), Plaza Ingeniero Torres Quevedo 1, 48013 Bilbao, Spain

[b] Dipartamento di Chimica Industriale "Toso Montanari", Alma Mater Studiorum, Universitá di Bologna, Viale del Risorgimento 4, 40136 Bologna, Italy

ARTICLE INFO

Keywords:
Bimetallic catalysts
Synthesis method
Ni-Cu interaction
HMF
BHMF
DMF
ZrO_2 support

ABSTRACT

The evident necessity to transition away from a reliance on fossil resources implies the need to produce high-value-added chemicals from non-conventional sources, such as lignocellulosic biomass. The cellulosic fraction of this resource can be converted into 5-hydroxymethylfurfural (HMF), which can be further transformed to 2,5-bis(hydroxymethyl)furan (BHMF), a polymeric precursor, or 2,5-dimethylfuran (DMF), serving as a substitute or additive of conventional gasoline. This work investigates the effect of the synthesis method of the Ni-Cu/ZrO_2 catalyst on the conversion of HMF to BHMF or DMF. The preparation process exerts influence on the dispersion of metals, the acidity of the catalyst, and the interaction of Ni-Cu. Consequently, product selectivity varied depending on the catalyst preparation method, with BHMF being the primary product when the catalyst was prepared through wet impregnation and DMF when precipitation was the chosen synthesis method. Concretely, a BHMF yield of 60 % yield was achieved at 150 °C with the impregnated catalyst, while a 65 % yield was obtained for DMF when employing the precipitation-prepared catalyst. Furthermore, a noticeable effect of the temperature on product selectivity was also detected.

Introduction

Today's energy crisis serves as a stark reminder of the fragility and unsustainable nature of our existing energy system. Despite recent efforts to increase investment in clean energy, founding remains insufficient to offer comprehensive solutions [1]. Concurrently, there is a pressing need to develop alternatives to products currently derived from fossil sources, particularly petroleum. In this context, biomass assumes an essential role in the production of high-value materials and composites, as it represents the sole renewable source capable of yielding such products [2].

Lignocellulosic biomass represents a promising resource due to its non-edible nature, abundant availability, low cost, and ready accessibility [3]. The three polymeric fractions of lignocellulosic biomass, namely lignin, cellulose and hemicellulose, are valorised for the production of valuable biofuel and biochemical [4]. Among these fractions, cellulose stands out as the most abundant, consisting of a linear chain of glucose units. This structural unit can undergo isomerization to yield fructose, which can subsequently be dehydrated to generate 5-hydroxymethylfurfural (HMF) [5].

HMF serves as compelling platform molecule for the synthesis of a diverse range of value-added compounds and biofuels [6], including 2, 5-bis(hydroxymethyl)furfural (BHMF) or 2,5 dimethylfuran (DMF). BHMF is derived from the selective hydrogenation of the C═O bond and garners significant interest due to its potential applications in the synthesis of functionalized polyethers, furanic polyamides and polyurethanes [7]. Conversely, the selective hydrodeoxygenation of HMF leads to the production of the liquid biofuel DMF, which boasts combustion properties and physical characteristics comparable to those of gasoline [8]. The reaction pathway has been extensively investigated and is summarized in Fig. 1.

Recent research has focused on the investigation of various catalyst parameters and their influence on catalytic activity. Huang et al. [9] conducted a study on monometallic Ni catalyst supported on carbon nanotubes, optimizing the NI content at 15 wt % to enhance BHMF production. Meanwhile, Hsiao et al. [10] concentrated on DMF

* Corresponding author at: Chemical and Environmental Engineering Department, Engineering Faculty of Bilbao, University of the Basque Country (UPV/EHU), Plaza Ingeniero Torres Quevedo 1, 48013 Bilbao, Spain.
E-mail address: nerea.viar@ehu.eus (N. Viar).

https://doi.org/10.1016/j.scenv.2023.100051
Received 30 May 2023; Received in revised form 7 November 2023; Accepted 19 November 2023
Available online 21 November 2023

production and developed monometallic Cu catalysts supported on different carbon carriers. Notably, the catalyst supported on a polymer-based spherical activated carbon (PBSAC) exhibited impressive results, with a 91.9 % HMF conversion and a 71.7 % DMF yield.

Furthermore, several authors have conducted investigations into the impact of various parameters on the production of both BHMF and DMF. Generally, bimetallic catalysts have demonstrated higher yields of the desired products when compared to monometallic catalysts. Zhao et al. [11] explored the variation in the Ni-Co ratio in a bimetallic catalyst for BHMF and DMF production. Their finding indicated that $Ni_{1.5}Co_{1.0}$ was the most active catalyst, delivering substantial yields of both products, with 93.1 % BHMF yield at a reaction temperature of 100 °C and 80.1 % of DMF yield at 200 °C.

In addition, Ahishakiye et al. [12] +investigated the reduction processś influence on the activity of a Co-CoOx-FeNiCo/γ-Al_2O_3 catalyst. The reduction temperature was found to impact the number of active metal sites and acid sites on the catalyst, consequently affection product selectivity. Specifically, the catalyst reduced at 300 °C exhibited greater selectivity for BHMF production, whereas the catalyst reduced at 500 °C favoured DMF production.

Given this background, this study aims to investigate the influence of the catalyst synthesis method on its activity and selectivity. The catalyst's preparation method is a critical factor that can alter its physicochemical properties, thereby affecting its selectivity. To address this, bimetallic Ni-Cu/ZrO_2 catalysts have been synthesized through wetness impregnation and precipitation methods. This work highlights how the catalyst's preparation method impacts its physicochemical properties, including the dispersion of active sites, total acidity, and the interaction between Ni and Cu. Furthermore, these effects of the synthesis process on the catalyst's properties also have repercussions on product selectivity.

Experimental

Catalyst preparation

Ni-Cu bimetallic catalysts supported on ZrO_2 were synthetized via wetness impregnation and precipitation methods. $ZrO(NO_3)\cdot H_2O$ (Sigma-Aldrich, 99 %), $Cu(NO_3)_2\cdot H_2O$ (Alfa Aesar, 98 %), and $Ni(NO_3)_2\cdot 6H_2O$ (Sigma Aldrich, 99.999 %) were employed as reagents. In both methods, 15 % of Ni and Cu was chosen as nominal weight.

The catalyst prepared via wetness impregnation was synthesized following a previously reported procedure [14]. Initially, Cu was impregnated using conventional wetness impregnation. The resulted solid was dried overnight and subsequently calcined in air at 250 °C for 2 h. Then, Ni was impregnated in a second step. The catalyst underwent another drying step under the same conditions. The synthetized catalyst was labelled as Ni-Cu/ZrO_2 WI.

The catalyst prepared through precipitation was also synthesized in two sequential steps. Initially, a solution of Zr and Cu nitrates was added dropwise into 100 ml of MiliQ water while the pH was maintained at a constant value of 9 through the addition of NH_4OH solution. After the nitrates solution had been added, the mixture was stirred at room temperature for 1 h. Subsequently, the temperature was raised to 60 °C, and the mixture was left at this temperature overnight to eliminate the water from the solution. The resulting product was then subjected to vacuum filtration until a pH of 7 was achieved, followed bu overnight drying. Lastly, the catalyst was calcined in air at 250 °C for 2 h. Following a similar procedure, Ni was precipitated in the subsequent step. The previously obtained solid was diluted in MiliQ water, and a solution of Ni nitrates was added dropwise while maintaining a pH of 9 through the addition of NH_4OH solution. The subsequent steps were identical to the first step explained above. The synthetized catalyst was labelled as Ni-Cu/ZrO_2 PR.

Finally, the Zr nitrates were calcined at 250 °C for 2 h to characterize the support.

Catalyst characterization

The catalysts were reduced at 275 °C at a rate of 5 °C/min for 2 h before the performance of some characterization techniques, such as temperature programmed desorption with ammonia, X-ray diffraction and X-ray photoelectron spectroscopy.

Textural properties

The calcined support and catalysts were outgassed at 150 °C for 4 h before the N_2 adsorption-desorption isotherms acquisition at −196 °C using Autosorb1C/TCD (Quantachrome, USA). The obtained isotherms were employed to calculate the BET surface area using the BET equation. The pore volume and average pore diameter were calculated by the Barrett-Joyner-Halenda (BJH) method.

Inductively coupled plasma optical emission spectroscopy (ICP-OES)

The catalysts were initially dissolved in an acidic solution (75 % HCl and 25 % HNO_3, in volume) by a microwave digestion system (Millestone ETHOS 1). Subsequently, the metal content was determined by ICP-OES (Perkin Elmer Optima 3000DV).

Temperature programmed desorption with ammonia (NH_3-TPD)

The acidity of the support and the catalysts was determined by AutoChem II Instrument (Micromeritics, USA) equipped with a TCD detector. The thermally treated samples were insitu reduced at 275 °C for 1 h, and the physisorbed impurities were removed by a He stream for 30 min. The samples were then cooled to 100 °C and NH_3 diluted in He (10 %) was fed to the sample for 30 min. The chemisorbed NH_3 was detected by TCD by heating the sample to 850 °C with He.

X-ray diffraction (XRD)

The X-ray diffraction patterns of the reduced catalysts were obtained using Seifert XRD 3000 diffractometer equipped with a PW 2200 Bragg-

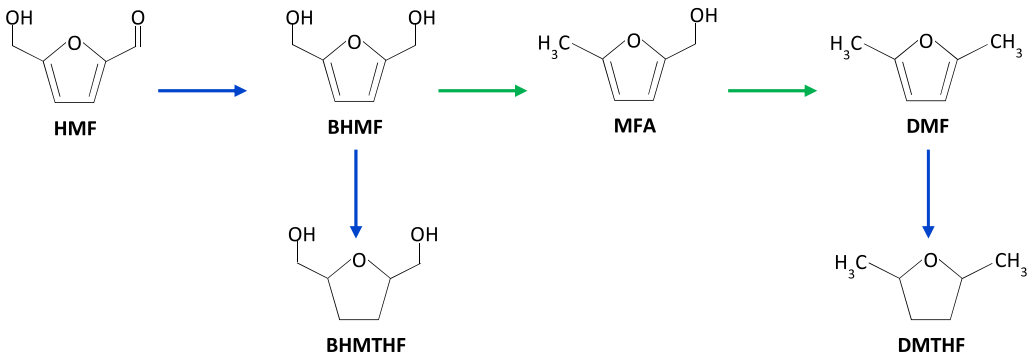

Fig. 1. Reaction pathway of HMF hydrogenation (blue) and hydrogenolysis (green) (adapted from [13]).

Brentano u/2 u goniometer, a bent graphite monochromator, and an automatic slit, using Cu K radiation (0.15418 nm) and 0.028° step size for scanning. The average crystallite size was calculated using Scherrer equation.

Temperature programmed reduction with hydrogen (H_2-TPR)

The reducibility of the catalysts was studied by AutoChem II Instrument (Micromeritics, USA) equipped with a TCD detector. The calcined catalysts were heated to 200 °C with Ar to desorb the physisorbed impurities. Then, the samples were cooled to 50 °C and again heated to 850 °C by flowing 5 % v/v H_2 diluted in Ar.

X-ray photoelectron spectroscopy (XPS)

The surface atomic ratios and oxidation state of the reduced catalysts was analysed using a VG Escalab 200 R spectrometer equipped with a hemispherical electron analyser and an Al K1 (h = 1486.6 eV) 120 W X-ray source. The samples were previously degassed at 200 °C. The spectrometer base pressure was typically 9–10 Torr. The spectra were collected with a pass energy of 20 eV.

Scanning transmission electron microscopy (STEM)

Elemental maps for the reduced catalysts were obtained to study the dispersion of the metals on the catalytic surface. A FEI Titan Gubed G2 60–300 transmission electron microscope at 300 kV was used, equipped with a Schottky X-FEG field emission electron gun, a monochromator, and a CEOS GmbH spherical aberration (C_s) corrector on the image side. On the other hand, a Super EDX system was used under a high-angle annular dark-field (HAADF) detector for Z contrast imaging under STEM conditions. In addition, EDX microanalyses were carried out with a Super-X EDX system, using a probe current of 240 pA and a semi-convergence angle of 10 mrad.

Activity and product analysis

The activity tests were carried out in 50 ml batch stainless steel Hastelloy reactors. Before the reaction catalysts were reduced at 275 °C at a rate of 5 °C/min for 2 h. 10 ml of HMF (Sigma-Aldrich, 99 %) diluted in 1-butanol (1.5 wt %) and 0.05 g of pre-reduced catalyst were placed in the reactor with a magnetic stirrer. The reactor was purged 3 times with N_2 and 3 times with H_2 at 20 bar and finally it was pressurized at desired pressure. The reaction was conducted at designed temperature under stirring. After the reaction, the products were filtrated and analysed by liquid and gas chromatography.

The reactant conversion and selectivity towards products were determined based on the following equations:

$$Conversion \quad (\%) = \left(1 - \frac{n^{t}_{HMF}}{n^{t=0}_{HMF}}\right) \cdot 100$$

$$Yield_i \quad (\%) = \left(\frac{n^{t}_{i}}{n^{t=0}_{HMF}}\right) \cdot 100$$

Results and discussion

Catalyst characterization results

Metallic content and textural properties

Metallic content and textural properties of thermally treated bare support and catalysts were determined by ICP-OES and N_2-physisorption, respectively, and are summarized in Table 1.

The metallic content of the catalysts was determined by ICP-OES, and the results are documented in Table 1. Notably, a higher metal content is discernible in the catalyst prepared through precipitation. Therefore, this method is preferable for metal incorporation. Furthermore, when comparing Ni content with Cu content, a higher concentration of Ni was observed in both samples, indicating a more effective loading of the metal introduced in the second step. This effect has been previously reported [14].

The surface area and pore volume experienced a significant reduction after the incorporation of Ni and Cu. The decline was more pronounced in the impregnated catalyst, suggesting a potentially lower dispersion of the metals within the catalyst support. Nevertheless, the average pore diameter exhibited an increase. This phenomenon could be attributed to the partial obstruction of the support's smaller pores due to the deposition of metals [15], resulting in the enlargement of the average pore diameter. These results align with the pore size distribution curves presented in Fig. S1. In the pore distribution, a difference is observed between the catalyst prepared through precipitation and the other samples. This difference was also observed in the isotherms plotted in Fig. S2.

Temperature programmed desorption with ammonia (NH_3-TPD)

The surface acidity of the bare support and the reduced catalysts determined by the temperature programmed desorption with ammonia are summarized in Table 1. ZrO_2 exhibited a larger surface area compared to the supported catalysts.

According to the literature [15,16], the decrease in acidity after the addition of the metals could be ascribed to the partial covering of the acidic sites on the support by metal clusters. This effect is more appreciable in Ni-Cu/ZrO_2 WI, which can be attributed to a lower dispersion of the metals, leading to the coverage of acidic sited by metallic clusters. This finding is consistent with the results obtained from N_2-physisorption analysis. To better understand the strength of the acidic species, NH_3-TPD curves are presented in Fig. S3. It can be observed that the catalyst prepared by precipitation exhibits peaks at higher temperatures, indicating the presence of stronger acidic sites when compared to the impregnated catalyst.

X-ray diffraction (XRD)

The X-ray diffraction patterns of the reduced catalysts are presented in Fig. 2. In both cases, a diffraction peak at 2θ = 31.3° was observed. This peak can be attributed to the presence of ZrO_2 crystals [17]. Notably, the diffraction peak of Ni-Cu/ZrO_2 WI appeared considerably broader in comparison to Ni-Cu/ZrO_2 PR, suggesting the formation of larger crystals. However, no other diffraction peaks associated with ZrO_2

Table 1
Metallic content, textural properties and surface acidity of bare support and catalysts.

	Metallic content[a]		Surface area[b] (m^2/g_{cat})	Pore volume[b] (cm^3/g_{cat})	Average pore diameter[b] (nm)	Desorbed NH_3[c] (mmol NH_3/g_{cat})
	Ni (%)	Cu (%)				
ZrO_2	-	-	137.6	0.26	7.2	0.39
Ni-Cu/ZrO_2 WI	11.5	8.0	12.3	0.03	10.0	0.11
Ni-Cu/ZrO_2 PR	13.8	10.5	25.6	0.09	8.9	0.19

Obtained from
[a] ICP-OES
[b] N_2-physisorption
[c] NH_3-TPD.

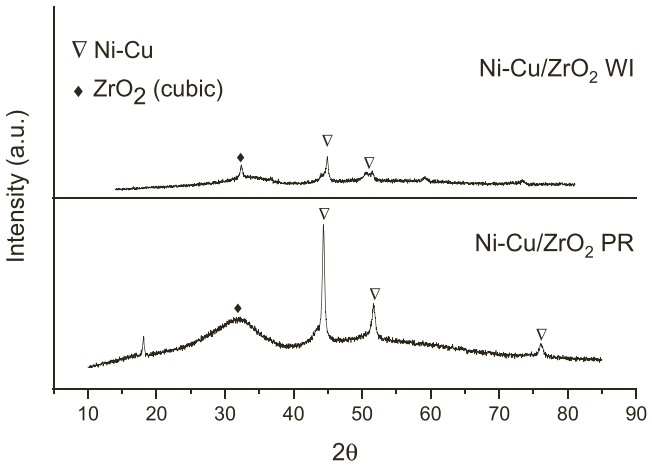

Fig. 2. XRD pattern for Ni-Cu/ZrO_2 catalysts.

were detected, indicating that the support is predominantly amorphous.

Distinct peaks corresponding to standard position of Cu (2θ = 43.316°, 50.448° and 74.124°, JCPDA Card No. 85–1326) or Ni (2θ = 44.496°, 51.849° and 76.381°, JCPDA Card No. 87–0712) were not detected. Nevertheless, the catalysts displayed diffraction peaks at 2θ = 43.8°, 51.0° and 75.9° [18]. Notably, these three peaks were observed to be positioned between the pure Cu and Ni diffraction peaks, indicating the potential presence of Ni-Cu crystallites.

In order to gain a deeper insight into the interaction between Ni and Cu, we conducted high-resolution analyses. The results obtained from these analysis are presented in Fig. 3. Additionally, the average crystallite sizes of Ni and Cu were calculated by Scherrer equation, and these values are tabulated in Table 2.

For the catalysts synthetized via wetness impregnation method, three distinct peaks were observed. The first peak is attributed to Cu-enriched crystals, while the last peak corresponds to Ni-enriched

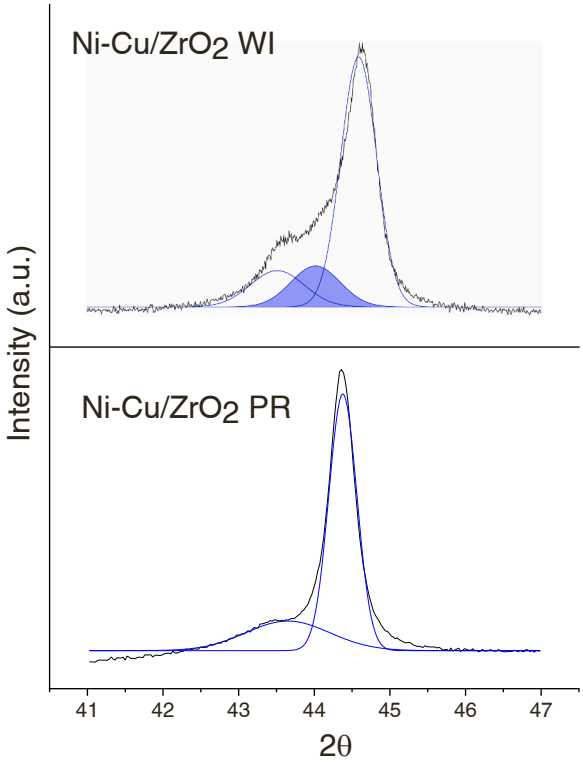

Fig. 3. High resolution XRD profiles.

Table 2
Crystallite size of reduced catalysts.

	No.	Crystallite size (nm)	Peak position (2θ)	Intensity (%)
Ni-Cu/ZrO_2 WI	Cu	10	43.6	25.1
	Ni/Cu	15	44.3	24.4
	Ni	25	44.6	50.5
Ni-Cu/ZrO_2 PR	Cu	5	43.4	27.1
	Ni	20	44.6	72.9

crystals. The intermediated peak likely corresponds to Ni-Cu crystals. In contrast, Ni-Cu/ZrO_2 PR catalyst exhibited only two peaks, associated with Cu-enriched and Ni-enriched crystals. These results confirm a stronger interaction between Ni and Cu when the catalyst is synthetized using the wetness impregnation method. This conclusion will be further discussed in H_2-TPR results.

In both instanced, the crystallite size of Ni-enriched crystals exceed that of Cu-enriched crystals. This phenomenon is likely attributed to the sequential impregnation process, wherein Cu was impregnated first, leading to a more effective dispersion of this metal on the support material.

Temperature programmed reduction with hydrogen (H_2-TPR)

To assess the reducibility of the catalysts and the interaction between Ni and Cu, H_2-TPR experiments were conducted. The profiles and their deconvolution are depicted in Fig. 4.

Based on the profiles obtained, it can be inferred that both catalysts are completely reduced at 275 °C. Consequently, the catalysts were reduced at this temperature prior to the activity tests. This reduction temperature is considerably lower than that observed for monometallic Ni catalyst examined in a prior study [14], which exhibited a broader reduction peak at higher temperatures in the range of 300–500 °C. These results suggest that the presence of Cu promoted the reducibility of Ni.

Upon deconvolution of both profiles, three distinct peaks were identified. The maximum temperature and the corresponding area percentages of each peak are detailed in Table 3. According to literature [19], it can be established that the initial and final peaks are associated with the reduction of Cu^{2+} and Ni^{2+}, respectively. The intermediate peak (highlighted in blue) may be attributed to the reduction of Ni-Cu

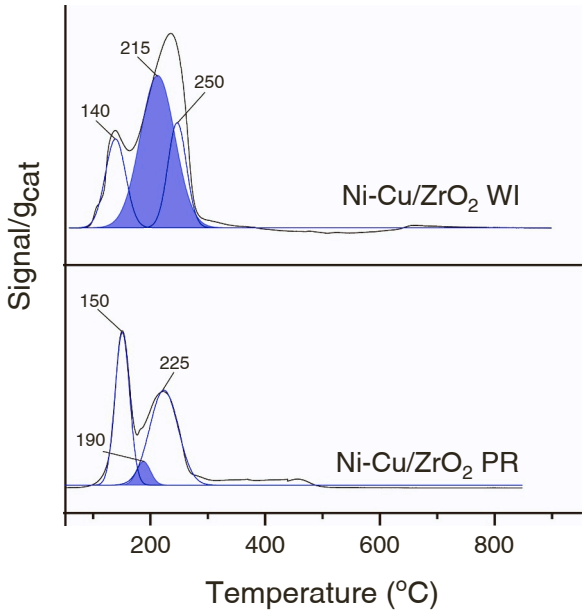

Fig. 4. H_2-TPR profiles for Ni-Cu/ZrO_2 catalysts.

Table 3
Maximum temperature and contribution in area (%) of deconvoluted H_2-TPR profiles.

	Cu		Ni/Cu		Ni	
	T (°C)	Area (%)	T (°C)	Area (%)	T (°C)	Area (%)
Ni-Cu/ZrO_2 WI	140	19	215	61	250	19
Ni-Cu/ZrO_2 PR	150	43	190	6	225	51

species.

A notable disparity exists between the two catalysts. In the sample prepared via wet impregnation, the primary peak is associated with the Ni-Cu interaction, whereas, in the sample prepared through precipitation, this peak exhibits minimal contribution. This observation aligns well with the findings from the X-ray diffraction analysis.

X-ray photoelectron spectroscopy (XPS)

The surface atomic ratios and oxidation states of the metals in the reduced catalysts were determined by X-ray photoelectron spectroscopy. The surface atomic ratios and oxidation states of reduced catalysts are tabulated in Table 4. These results indicated an increase in the Cu/Zr and Ni/Zr ratios when the catalyst was synthetized by precipitation method. This could be attributed to the better dispersion of this catalyst, as evidenced in the N_2-physisorption and NH_3-TPD results.

Additionally, it is noteworthy that Ni-Cu/ZrO_2 PR displayed elevated metallic Ni and Cu ratios. The better dispersion of the metals could be promoting the reduction of these elements, thereby, enhancing the metallic state of Ni and Cu.

Furthermore, the fitted spectra XPS spectra are presented in Fig. S4. The binding energies (BE) corresponding to Ni and Cu were Ni $2p_{3/2}$ and Cu $2p_{3/2}$, respectively. The presence of the satellite peak in the Cu $2p_{3/2}$ and in the Ni $2p_{3/2}$ spectra indicated the presence of Cu^{2+} (peak at 940.4 eV) and Ni^{2+} (861.3 eV) species on the surface of the Ni-Cu/ZrO_2 WI catalyst. The presence of Cu^{+} was additionally verified by the detection of CuLMM peak at binding energy of 569.2 eV. Moreover, the presence of metallic Cu (938.8 eV) and Ni (859.0 eV) was confirmed.

Kishi and Fujita [20] identified the binding energy observed at 821.3 eV, 853.8 eV and 855.8 eV as characteristic of Ni-Cu alloy. Interestingly, the impregnated catalyst exhibited a peak at 854.0 eV, which can also be ascribed to the Ni-Cu alloy. These authors have further suggested that Cu species y present as predominantly exist in the form of a Cu-Ni alloy, with binding energy of 932.3 eV [21]. Consequently, the presence of a peak at 932.4 eV can be indicative of the existence of a Ni-Cu alloy on the ZrO_2 surface. These findings are in good agreement with the previously mentioned XRD and H_2-TPR results.

In the case of the Ni-Cu/ZrO_2 PR catalyst, the absence of satellite peaks in the Cu $2p_{3/2}$ spectrum indicated the presence of only Cu^0 and Cu^{+} species on the catalytic surface. The presence of Cu^{+} was substantiated by the detection of CuLMM peak at 568.3 eV. Furthermore, the peak observed in the Cu $2p_{3/2}$ spectrum 932.6 eV does not imply the presence of Ni-Cu alloy, in contrast to the impregnated catalyst, as previously reported by Kishi and Sasanuma [21]. This observation is corroborated by the Ni $2p_{3/2}$ spectrum, where no peaks indicative of Ni-Cu alloy formation were discerned. In this spectrum, only two peaks were evident, associated with Ni^0 and Ni^{2+}. The presence of the latter species was confirmed by the presence of satellite peaks. There results align consistently with the preceding findings.

Table 4
Surface atomic ratios and oxidation states of reduced catalysts.

	Surface atomic ratios and oxidation states			
	Cu/Zr	Cu^0 /Zr	Ni/Zr	Ni^0 /Zr
Ni-Cu/ZrO_2 WI	0.57	0.34	0.54	0.10
Ni-Cu/ZrO_2 PR	0.88	0.44	1.24	0.38

Obtained from XPS.

Scanning transmission electron microscopy (STEM)

The elemental maps for the reduced catalysts (depicted in Fig. 5) were acquired using STEM, allowing for the examination of metal dispersion on the support. These elemental maps demonstrate a favourable dispersion of the metals on the catalytic support in both samples. However, it is noteworthy that the catalyst synthesized via the precipitation method exhibits a notably superior dispersion of Ni, in accordance with the results obtained through XPS.

Activity results

The synthesized catalysts were tested in 50 ml stainless steel autoclaves. Initially, the experimental conditions, including temperature and pressure, were examined, along with the product distribution over time, using Ni-Cu/ZrO_2 WI catalysts. Subsequently, the Ni-Cu/ZrO_2 PR catalyst was tested under optimized operational conditions. The physicochemical properties determined by different characterization techniques are important for the comprehension of variations in activity.

Effect of the hydrogen pressure

Hydrogen pressure represents a crucial parameter in hydrogenolysis reactions. Tzeng et al. [22] have previously concluded that there exists a pressure threshold beyond which any further increase does not contribute to the enhancement of hydrogenation and hydrogenolysis reactions. In an effort to investigate this pressure limit within the catalytic system, the pressure was elevated from 15 bar to 30 bar, and the results are depicted in Fig. 6.

When increasing the pressure from 15 to 30 bar, similar activity results were observed. Consequently, it is evident that the pressure increase does not intensify the hydrogenolysis reactions. As a result, a hydrogen pressure of 15 bar of was selected for subsequent experiments.

Effect of the temperature

In order to understand the influence of the temperature in the hydrogenation of HMF to DMF, this parameter was increased from 50° to 225°C, while maintaining a constant hydrogen pressure of 15 bar, for 5 h. The obtained results are illustrated in Fig. 7.

The temperature variation exhibited interesting results. At lower temperature (50 °C), conversion was negligible. An increase in temperature up to 100 °C evidenced the necessity for higher temperature to facilitate the conversion of HMF and the hydrogenation of the aldehyde group into BHMF. Further rise of the temperature promoted the hydrogenation of the –C═O bond, resulting in a BHMF yield of approximately 60 % at 150 °C. Additionally, the production of BHMTHF was observed, involving the hydrogenation of the furan ring of BHMF. However, hydrogenolysis products were hardly detected. These results suggest that, at this temperature, hydrogenation reactions are favoured, while hydrogenolysis reactions are not as prominent.

Elevated temperatures implied the formation of MFA, DMF and DMTHF, which result from the hydrogenolysis of BHMF. These results suggest that higher temperatures are needed to promote hydrogenolysis reactions, aligning with the findings reported by Pomeroy et al. [23]. Moreover, the yield of BHMTHF increased with rising temperature, while the production of BHMF decreased. Consequently, higher temperature also enhance the hydrogenation of the furan ring.

Nonetheless, as the temperature increased, the overall product yield decreased, indicating a decline in carbon balance. A similar effect was observed by Li et al. [24]. The higher temperature may likely induce the formation of undesirable degradation products. Thus, it is essential to develop an efficient catalytic system capable of preventing the generation of degradation products at elevated temperatures.

Product distribution over time

To better understand the reaction pathway, the product distribution over time was studied at 225 °C and 15 bar of H_2, and the results are presented in Fig. 8. Complete conversion of HMF conversion was

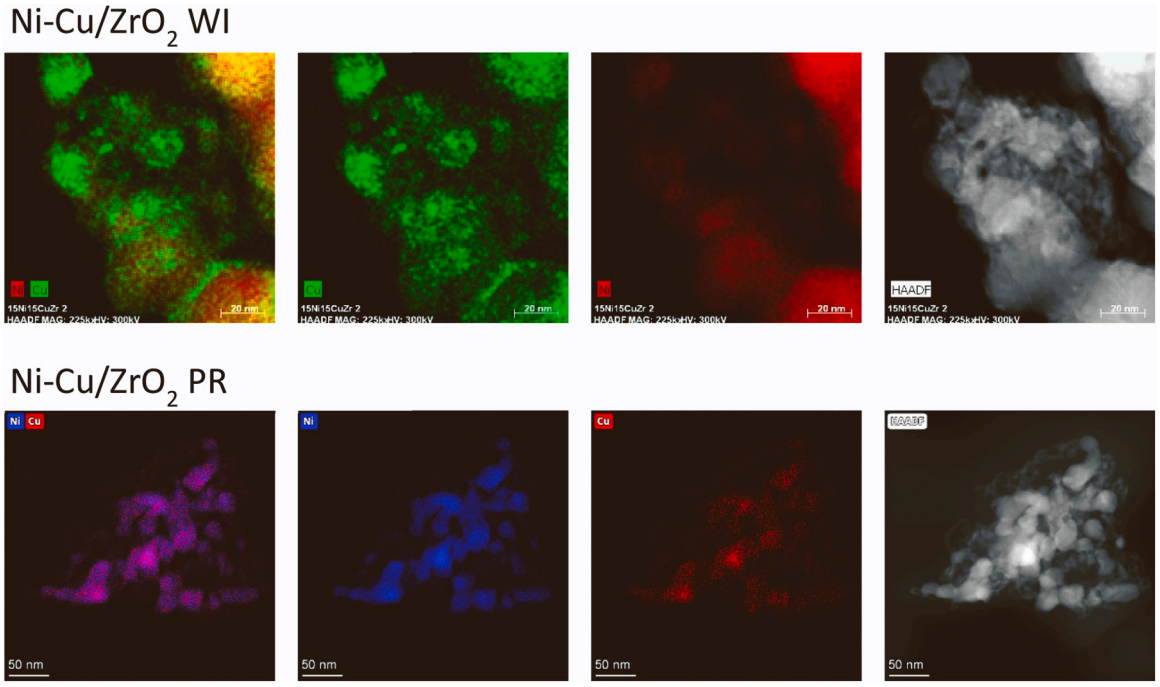

Fig. 5. STEM images of reduced catalysts.

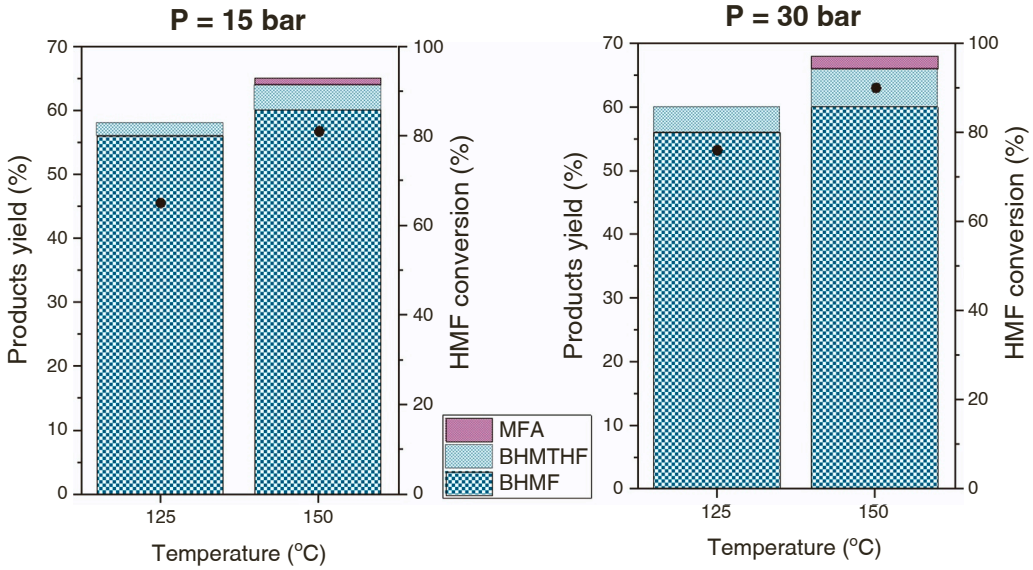

Fig. 6. HMF conversion (•) and products yield for Ni-Cu/ZrO_2 WI for 5 h at different temperature and pressure conditions: (a) 15 bar of H_2; (b) P = 30 bar of H_2. Reaction conditions: 1.5 wt % HMF in 1-butanol (10 ml).

achieved within 3 h. However, the product distribution evolved over time. During the first hour of the reaction, over 50 % of the total product yield was attained, with the observation of both hydrogenation and hydrogenolysis products. Extending the reaction time to 3 h led to an increase in the hydrogenation products, such as BHMF and BHMTHF. Furthermore, while the yield of MFA exhibited a slight declined, the yield of DMF gradually increased, indicating a preference for the hydrogenolysis of the hydroxyl group.

Nonetheless, the extended reaction time to 5 h resulted in a reduction of the overall product yield, signifying a decrease in carbon balance. BHMF was not detected, indicating its complete conversion to generate both BHMTHF through the hydrogenation of the furan ring and MFA via the hydrogenolysis of the hydroxyl group, which was subsequently converted into DMF. Additionally, the presence of DMTHF was observed, possibly arising from the hydrogenation of the furan ring of DMF.

Effect of the catalyst synthesis method

The Ni-Cu/ZrO_2 PR catalyst was tested varying the reaction temperature, and the obtained results are presented in Fig. 9. The temperature i is similar to that one observed for Ni-Cu/ZrO_2 WI. Lower temperature involved low conversion and BHMF yield, a product resulting from the hydrogenation of the aldehyde group. Higher temperatures lead to the production of MFA and DMF, indicating the hydrogenolysis of the hydroxyl group. As temperature increases, the production of BHMF diminishes, while the yield of DMF is rises. The

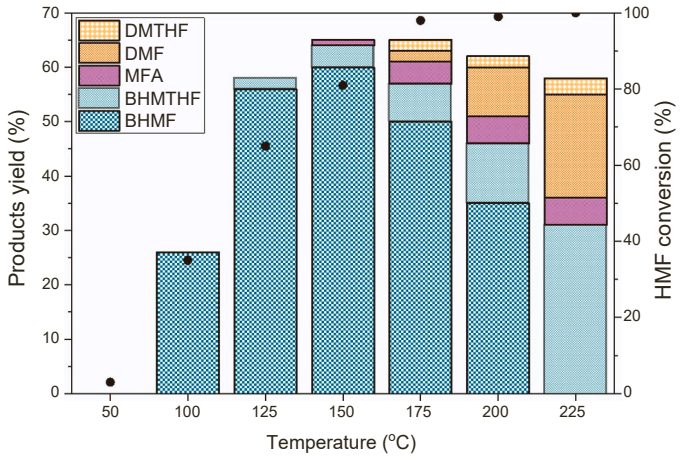

Fig. 7. HMF conversion (•) and products yield for Ni-Cu/ZrO_2 WI at 15 bar of H_2 for 5 h at different temperature conditions. Reaction conditions: 1.5 wt % HMF in 1-butanol (10 ml).

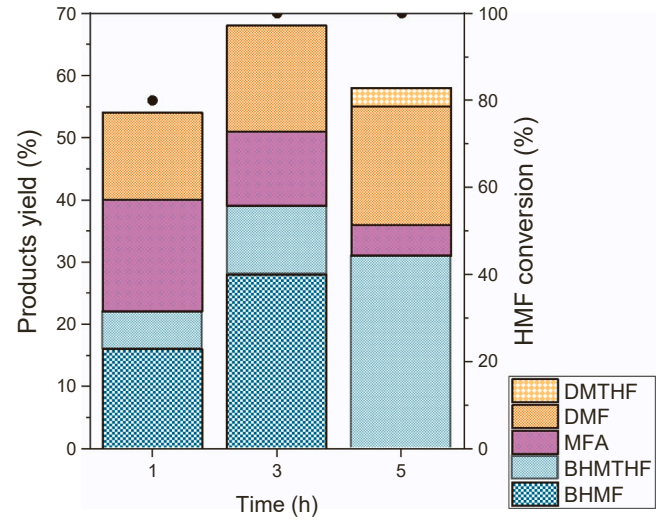

Fig. 8. HMF conversion (•) and products yield for Ni-Cu/ZrO_2 WI at 15 bar of H_2 and 225 °C. Reaction conditions: 1.5 wt % HMF in 1-butanol (10 ml).

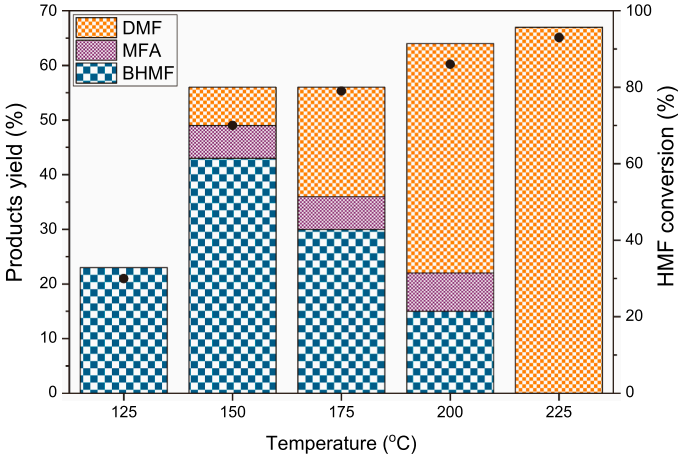

Fig. 9. HMF conversion (•) and products yield for Ni-Cu/ZrO_2 PR at 15 bar of H_2 for 5 h at different temperature conditions. Reaction conditions: 1.5 wt % HMF in 1-butanol (10 ml).

maximum DMF yield reaches nearly 70 % at 220 °C. Importantly, the DMF yield does not decline with increasing temperature, suggesting that the production of degradation compounds is not favoured.

In comparison to the catalyst synthesized via wet impregnation (refer to Fig. 7), HMF conversion is lower across all temperatures for the Ni-Cu/ZrO_2 PR catalyst. Consequently, Ni-Cu/ZrO_2 PR exhibits lower catalytic activity compared to Ni-Cu/ZrO_2 WI. This fact can likely be attributed to the lower Ni-Cu interaction, as observed in XRD and H_2-TPR analysis. However, the high activity of Ni-Cu species possibly could be contributing to the generation of degradation products observed at elevated temperatures in the impregnated Ni-Cu/ZrO_2 WI. In contrast, despite the absence of high Ni-Cu interaction in Ni-Cu/ZrO_2 PR, the catalyst demonstrates a significant high activity. This may be associated with the superior dispersion and higher metallic Ni and Cu content on the catalyst surface.

Another important observation is that the catalyst synthetized through wet impregnation exhibited higher hydrogenation activity, while the catalyst prepared via precipitation appeared to be more effective in the hydrogenolysis of the C-O bond, resulting in a more efficient production of DMF. This result may be related to the variation in acidity, and therefore, the number of acid sites, as revealed by NH_3-TPD. It has been previously reported [25] that acid sites enhance the hydrogenolysis of C−OH during HMF conversion. Moreover, it has been recently reported that strong acidic sites promote the hydrogenolysis of C-O bond [26]. This could account for the elevated DMF production in the Ni-Cu/ZrO_2 PR catalyst, characterized by a notable presence of strong acidic sites in the NH_3-TPD analysis. In this work, Ni-Cu/ZrO_2 PR exhibited higher acidity than Ni-Cu/ZrO_2 WI, which is associated with the better dispersion observed in this catalyst. The high acidity is likely linked to enhanced activity in cleaving C-O bonds, leading to a higher DMF yield. Moreover, the catalyst synthetized through precipitation does not exhibit activity in promoting the hydrogenation of the furanic ring, implying that neither BHMTHF nor DMTHF were produced with this catalyst.

Recently, similar studies have revealed that the most significant factor in the production of BHMF and/or DMF is the balance between metallic sites and acidic sites [11,12,27]. These studies have also reported high conversion and favourable product yields. Specifically, 93.1 % BHMF selectivity and 80.1 % DMF selectivity was achieved with a nickel based bimetallic $Ni_{1.5}Co_1$ catalyst [11]. Nevertheless, while the effect of metal loading has been exposed in all these studies, none of them delved into an examination of the preparation method.

Conclusions

The temperature has been determined to exert a significant influence on product distribution. The catalyst demonstrates the capability to hydrogenate the aldehyde group of HMF at relatively low temperatures, around 150 °C. However, higher temperatures are necessary for the cleavage of the C−O bond, a crucial step for the production of DMF. Therefore, the temperature can be optimized based on the desired product.

The difference in physicochemical properties was evidenced in the activity results. The Ni-Cu interaction observed in Ni-Cu/ZrO_2 WI likely enhanced the conversion of HMF. Furthermore, the high activity of this phase may contribute to the generation of undesired degradation products when the temperature is raised to 225 °C. The total product yield after 3 h of reaction reached approximately 70 %, with nearly 60 % of the obtained products arising from the hydrogenation of both the aldehyde group and the furanic ring. However, the cleavage of C−O bond was less noticeable, resulting in lower yields of MFA, DMF and DMTHF.

Conversely, Ni-Cu/ZrO_2 PR exhibited a high selectivity for DMF production at a temperature of 225 °C, which could be attributed to the elevated acidity observed in the NH_3-TPD analysis. Consequently, achieving a favourable balance between metallic active sites and acidic

sites is crucial for the hydrogenolysis of HMF to produce DMF.

Funding sources

This research was supported by the University of the Basque Country (UPV/EHU), Basque Government (IT1554-22), and the Spanish Ministry of Economy, Industry and Competitiveness (PID2021-122736OB-C43).

CRediT authorship contribution statement

The manuscript was written through contributions of all authors. All authors have given approval to the final version of the manuscript.

Declaration of Competing Interest

The authors declare the following financial interests/personal relationships which may be considered as potential competing interests: Jesus M. Requies reports financial support was provided by University of the Basque Country Superior Technical School of Engineering of Bilbao.

Data Availability

No data was used for the research described in the article.

Acknowledgments

The authors thank for technical and human support provided by SGIker of UPV/EHU and European funding (ERDF and ESF).

Appendix A. Supporting information

Supplementary data associated with this article can be found in the online version at doi:10.1016/j.scenv.2023.100051.

References

[1] I.E. Agency, International Energy Agency (IEA) World Energy Outlook 2022, (2022).
[2] C.C. Truong, V.K. Verma, P. Mishra, Y.W. Suh, D.K. Mishra, Catalytic transformation of biomass-based feedstocks in green solvents, INC (2022), https://doi.org/10.1016/B978-0-12-824419-7.00004-2.
[3] W. Deng, Y. Feng, J. Fu, H. Guo, Y. Guo, B. Han, Z. Jiang, L. Kong, C. Li, H. Liu, P.T. T. Nguyen, P. Ren, F. Wang, S. Wang, Y. Wang, Y. Wang, S.S. Wong, K. Yan, N. Yan, X. Yang, Y. Zhang, Z. Zhang, X. Zeng, H. Zhou, Catalytic conversion of lignocellulosic biomass into chemicals and fuels, Green. Energy Environ. 8 (2022) 10–114, https://doi.org/10.1016/j.gee.2022.07.003.
[4] V. Ashokkumar, R. Venkatkarthick, S. Jayashree, S. Chuetor, S. Dharmaraj, G. Kumar, W.H. Chen, C. Ngamcharussrivichai, Recent advances in lignocellulosic biomass for biofuels and value-added bioproducts - a critical review, Bioresour. Technol. 344 (2022), 126195, https://doi.org/10.1016/j.biortech.2021.126195.
[5] H. Xu, X. Li, W. Hu, L. Lu, J. Chen, Y. Zhu, H. Zhou, C. Si, Recent advances on solid acid catalyic systems for production of 5-Hydroxymethylfurfural from biomass derivatives, Fuel Process. Technol. 234 (2022), 107338, https://doi.org/10.1016/j.fuproc.2022.107338.
[6] H. Son Le, Z. Said, M. Tuan Pham, T. Hieu Le, I. Veza, V. Nhanh Nguyen, B. Deepanraj, L. Huong Nguyen, Production of HMF and DMF biofuel from carbohydrates through catalytic pathways as a sustainable strategy for the future energy sector, Fuel 324 (2022), 124474, https://doi.org/10.1016/j.fuel.2022.124474.
[7] J. Wang, J. Zhao, J. Fu, C. Miao, S. Jia, P. Yan, J. Huang, Applied catalysis A, general highly selective hydrogenation of 5-hydroxymethylfurfural to 2, 5-bis (hydroxymethyl) furan over metal-oxide supported Pt catalysts: the role of basic sites, Appl. Catal. A Gen. 643 (2022), 118762, https://doi.org/10.1016/j.apcata.2022.118762.
[8] K.I. Galkin, V.P. Ananikov, When Will 5-Hydroxymethylfurfural, the " Sleeping Giant " of Sustainable Chemistry, Awaken ?, (n.d.). https://doi.org/10.1002/cssc.201900592.
[9] Z. Huang, X. Sun, W. Zhao, X. Zhu, Z. Zeng, Q. Xu, X. Liu, methyl) furan using carbon nanotubes-supported nickel catalysts, 5 (2022) 289–298.
[10] Y.W. Hsiao, X. Zong, J. Zhou, W. Zheng, D.G. Vlachos, Selective hydrodeoxygenation of 5-hydroxymethylfurfural (HMF) to 2,5-dimethylfuran (DMF) over carbon supported copper catalysts using isopropyl alcohol as a hydrogen donor, Appl. Catal. B 317 (2022), 121790, https://doi.org/10.1016/j.apcatb.2022.121790.
[11] W. Zhao, Z. Huang, L. Yang, X. Liu, H. Xie, Z. Liu, Highly efficient syntheses of 2,5-bis(hydroxymethyl)furan and 2.5-dimethylfuran via the hydrogenation of biomass-derived 5-hydroxymethylfur fural over a nickel – cobalt bimetallic catalyst, Appl. Surf. Sci. 577 (2022), 151869, https://doi.org/10.1016/j.apsusc.2021.151869.
[12] R. Ahishakiye, F. Wang, X. Zhang, M. Sun, Y. Zhai, Y. Liu, Y. Wu, M. Li, M. Li, Q. Zhang, Novel noble metal-free and recyclable Co-CoOx-FeNiCo/γ-Al2O3 catalyst for selective hydrogenation of 5-hydroxymethylfurfural to 2,5-dimethylfuran or 2,5-Bis(hydroxymethyl)furan, Chem. Eng. J. 450 (2022), 138187, https://doi.org/10.1016/j.cej.2022.138187.
[13] L. Hu, L. Lin, S. Liu, Chemoselective hydrogenation of biomass-derived 5-hydroxymethylfurfural into the liquid biofuel 2,5-dimethylfuran, Ind. Eng. Chem. Res 53 (2014) 9969–9978, https://doi.org/10.1021/ie5013807.
[14] N. Viar, J.M. Requies, I. Agirre, A. Iriondo, M. Gil-Calvo, P.L. Arias, Ni-Cu bimetallic catalytic system for producing 5-hydroxymethylfurfural-derived value-added biofuels, ACS Sustain Chem. Eng. 8 (2020) 11183–11193, https://doi.org/10.1021/acssuschemeng.0c02433.
[15] I.C.A. Souza, R.L. Manfro, M.M.V.M. Souza, Hydrogen production from steam reforming of acetic acid over Pt–Ni bimetallic catalysts supported on ZrO2, Biomass. Bioenergy 156 (2022), 106317, https://doi.org/10.1016/j.biombioe.2021.106317.
[16] M.H.O. Nunes, V.T. Da Silva, M. Schmal, The effect of copper loading on the acidity of Cu/HZSM-5 catalysts: IR of ammonia and methanol for methylamines synthesis, Appl. Catal. A Gen. 294 (2005) 148–155, https://doi.org/10.1016/j.apcata.2005.06.031.
[17] M.K. Shukla, Y. Balyan, A. Kumar, T. Bhaskar, A. Dhar, Catalytic oxidation of soot by CeO2–ZrO2 catalysts: role of Zr, Mater. Chem. Phys. 286 (2022), 126161, https://doi.org/10.1016/j.matchemphys.2022.126161.
[18] B. Gao, J. Zhang, J.H. Yang, Bimetallic Cu-Ni/MCM-41 catalyst for efficiently selective transfer hydrogenation of furfural into furfural alcohol, Mol. Catal. 517 (2022), 112065, https://doi.org/10.1016/j.mcat.2021.112065.
[19] M. Khzouz, E.I. Gkanas, S. Du, J. Wood, Catalytic performance of Ni-Cu/Al2O3 for effective syngas production by methanol steam reforming, Fuel 232 (2018) 672–683, https://doi.org/10.1016/j.fuel.2018.06.025.
[20] K. Kishi, T. Fujita, Interaction of Ni/Cu (100) surfaces with O2 studied by XPS, Surf. Sci. 227 (1990) 107–113.
[21] K. Kishi, M. Sasanuma, The interaction of O2 with Cu/Ni(100) and Cu/NiO/Ni (100) surfaces studied by XPS, J. Electron Spectros Relat. Phenom. 48 (1989) 421–434.
[22] T.W. Tzeng, C.Y. Lin, C.W. Pao, J.L. Chen, R.J.G. Nuguid, P.W. Chung, Understanding catalytic hydrogenolysis of 5-hydroxymethylfurfural (HMF) to 2,5-dimethylfuran (DMF) using carbon supported Ru catalysts, Fuel Process. Technol. 199 (2020), 106225, https://doi.org/10.1016/j.fuproc.2019.106225.
[23] B. Pomeroy, M. Grilc, S. Gyergyek, B. Likozar, Catalyst structure-based hydroxymethylfurfural (HMF) hydrogenation mechanisms, activity and selectivity over Ni, Chem. Eng. J. 412 (2021), https://doi.org/10.1016/j.cej.2020.127553.
[24] J. Li, H. Liu, Z. An, Y. Kong, L. Huang, D. Duan, R. Long, P. Yang, Y.Y. Jiang, J. Liu, J. Zhang, T. Wan, J. Fu, R. Pan, X. Wang, D.G. Vlachos, Nitrogen-doped carbon for selective pseudo-metal-free hydrodeoxygenation of 5-hydroxymethylfurfural to 2,5-dimethylfuran: Importance of trace iron impurity, J. Catal. 417 (2023) 396–407, https://doi.org/10.1016/j.jcat.2022.12.021.
[25] D. Wu, S. Zhang, W.Y. Hernández, W. Baaziz, O. Ersen, M. Marinova, A. Y. Khodakov, V.V. Ordomsky, Dual metal-acid Pd-Br catalyst for selective hydrodeoxygenation of 5-hydroxymethylfurfural (HMF) to 2,5-dimethylfuran at ambient temperature, ACS Catal. 11 (2021) 19–30, https://doi.org/10.1021/acscatal.0c03955.
[26] K. Cui, X. Zhao, Q. Peng, H. Gong, X. Wei, J. Wang, M. Chen, Z. Hou, Catalytic transfer hydrogenolysis of C–O bonds in lignin model compounds without arene hydrogenation, Green. Chem. Eng. 3 (2022) 25–33, https://doi.org/10.1016/j.gce.2021.07.008.
[27] Y. Yu, H. Liu, J. Zhang, H. Zhang, Y. Sun, L. Peng, Highly efficient, amorphous bimetal Ni-Fe borides-catalyzed hydrogenolysis of 5-hydroxymethylfurfural into 2,5-dimethylfuran, Renew. Energy 209 (2023) 453–461, https://doi.org/10.1016/j.renene.2023.04.023.